The *c-Myc* Oncogene Maintains Corneal Epithelial Architecture at Homeostasis, Modulates p63 Expression, and Enhances Proliferation During Tissue Repair

Céline Portal,[1] Zheng Wang,[2] Donald K. Scott,[3] J. Mario Wolosin,[2] and Carlo Iomini[1,4]

[1]Department of Ophthalmology, Wilmer Eye Institute, Johns Hopkins University School of Medicine, Baltimore, Maryland, United States
[2]Department of Ophthalmology, Icahn School of Medicine at Mount Sinai, New York, New York, United States
[3]Department of Medicine, Icahn School of Medicine at Mount Sinai, New York, New York, United States
[4]Department of Cell Biology, Johns Hopkins University School of Medicine, Baltimore, Maryland, United States

Correspondence: J. Mario Wolosin, Department of Ophthalmology, Icahn School of Medicine at Mount Sinai, Box1183, One Gustave L. Levy Place, New York, NY 10029, USA; jmario.wolosin@mssm.edu.
Carlo Iomini, Department of Ophthalmology, Wilmer Eye Institute, Johns Hopkins University School of Medicine, 400 N. Broadway, Baltimore, MD 21205, USA; ciomini1@jhmi.edu.

Received: August 10, 2021
Accepted: January 5, 2022
Published: February 1, 2022

Citation: Portal C, Wang Z, Scott DK, Wolosin JM, Iomini C. The *c-Myc* oncogene maintains corneal epithelial architecture at homeostasis, modulates p63 expression, and enhances proliferation during tissue repair. *Invest Ophthalmol Vis Sci.* 2022;63(2):3. https://doi.org/10.1167/iovs.63.2.3

Purpose. The transcription factor c-Myc (Myc) plays central regulatory roles in both self-renewal and differentiation of progenitors of multiple cell lineages. Here, we address its function in corneal epithelium (CE) maintenance and repair.

Methods. Myc ablation in the limbal–corneal epithelium was achieved by crossing a floxed *Myc* mouse allele ($Myc^{fl/fl}$) with a mouse line expressing the Cre recombinase gene under the keratin (Krt) 14 promoter. CE stratification and protein localization were assessed by histology of paraffin and plastic sections and by immunohistochemistry of frozen sections, respectively. Protein levels and gene expression were determined by western blot and real-time quantitative PCR, respectively. CE wound closure was tracked by fluorescein staining.

Results. At birth, mutant mice appeared indistinguishable from control littermates; however, their rates of postnatal weight gain were 67% lower than those of controls. After weaning, mutants also exhibited spontaneous skin ulcerations, predominantly in the tail and lower lip, and died 45 to 60 days after birth. The mutant CE displayed an increase in stratal thickness, increased levels of Krt12 in superficial cells, and decreased exfoliation rates. Accordingly, the absence of Myc perturbed protein and mRNA levels of genes modulating differentiation and proliferation processes, including $\Delta Np63\beta$, *Ets1*, and two Notch target genes, *Hey1* and *Maml1*. Furthermore, Myc promoted CE wound closure and wound-induced hyperproliferation.

Conclusions. Myc regulates the balance among CE stratification, differentiation, and surface exfoliation and promotes the transition to the hyperproliferative state during wound healing. Its effect on this balance may be exerted through the control of multiple regulators of cell fate, including isoforms of tumor protein p63.

Keywords: corneal epithelium, corneal wound healing, c-Myc

The epidermis and other ectoderm-derived stratified epithelia function as a barrier of solute or pathogen infiltration. This function depends on (1) the capacity to rapidly expand the cell population and migrate to seal any externally generated interruption of the epithelial continuum, and (2) the proper, stepwise maturation of the epithelial cells as they progress from the base to the apical strata locations. These functions are supported by a general plan for self-renewing tissues that is based on the existence of long-lived, rare populations of stem cells (SCs) localized at specialized basal niches.[1–4] The SCs give rise to rapidly proliferating cells within the basal compartment at slow rates under steady-state conditions or at accelerated rates when the environmental conditions require it (e.g., during CE repair). After a number of cycles, these latter cells initiate their terminal differentiation (TD) program and hence are referred to as transiently amplifying cells (TACs). Thus, the SC–TAC–TD balance underpins the status of many tissues, including the epidermis, stratified epithelium of the cornea,[5] simple columnar epithelium of the gastrointestinal tract[6,7] and hematopoietic system.[8] The specific TD paths confer to each of these tissues its specific nature or phenotype.

The oncogene *c-Myc* (*Myc*) has emerged as a critical factor in the control of the balance between SC and TAC. In mice epidermis[9–11] and the hematopoietic system,[12,13] *Myc* overexpression causes extemporal SC proliferation with the promotion of SC-to-TAC transition. This is poised to result in gradual exhaustion of the SC population. In the epidermis, excess *Myc* accelerates the rate of TAC generation, which leads to an abnormal accumulation of cells in the final stages of terminal differentiation.[11,14] On the other hand, ablation of *Myc* is also disruptive. In the hematopoietic system, it prevents the SC-to-TAC transition, resulting in the

accumulation of SCs within the bone marrow with a concomitant decrease in the ability by the blood progenitor cells to generate critical blood lineage precursors.[12,15,16] Due to what are likely to be similar Myc effects in stratified epithelia, conditional knockout mice in which Myc was constitutively ablated in keratin (Krt) 5–expressing tissues, the skin becomes thin and fragile, tearing off in areas of mechanical friction.[17] The skin of these mice also displayed long-healing spontaneous lesions and delayed healing capability following a mechanical wound.[17] Intriguingly, in other constantly self-renewing epithelia such as the intestine, the absence of Myc seems to be inconsequential for the homeostasis of the mature intestinal epithelium.[18] Thus, it remains conceptually challenging to reconcile the contrasting function of Myc opposing concurrent pro-growth and pro-differentiative effects in different tissues.

The corneal epithelium (CE) is a fast-renewing epithelium of ectodermal origin. Two of the most distinctive features are the segregation of SCs to the limbal region[19–22] and the divergence of terminal differentiation from the keratinized or *para*-keratinized, denucleated phenotype, characteristic of most stratified epithelia, to a fully keratinization-free, secretory epithelial phenotype.[23,24] These distinct characteristics make this tissue a unique paradigm to address the role of Myc in maintaining the balance among SC, TAC, and the TD cell compartments. Prior studies inducing gain or loss of *Myc* function in ectoderm-derived epithelia in mice via the *Krt5* promoter did not investigate the phenotype of the *Krt5*-positive ocular surface epithelia.[9,17] Thus, we generated a *Myc* knockout mouse for tissues expressing *Krt14*, a gene co-expressed with *Krt5* in all stratified epithelia. Our studies demonstrate that, in the limbal corneal epithelium, Myc plays a major role in the activation of precursor cell proliferation and a subtle but consequential role in the coordination of cellular maturation during the stratification of terminally differentiated cells. Biochemical studies have identified the overexpression of isoforms of the tumor protein p63 (*TP63*) and the differentiation-associated gene *Ets1*, as well as *Hey1* and *Maml1*, two Notch target genes, as potential mediators of these effects.

Materials and Methods

Generation of Krt14 Conditional Knockout Mice

The mouse strain *Myc*^{tm2Fwa}, here referred to as *Myc*$^{fl/fl}$,[25] maintained in a FVB genetic background was outcrossed to the *Tg(KRT14-cre)1Amc/J* strain (here referred to as *K14-cre*), obtained from The Jackson Laboratory (018964; Bar Harbor, ME, USA)[26] maintained on mixed C57BL/6 and 129 genetic backgrounds. F1 siblings were intercrossed or backcrossed to *Myc*$^{fl/fl}$ to obtain the desired mutant genotype. Thus, littermates had a mixed background resulting in a white, brown, or black coat color. Genotypes other than *K14-cre; Myc*$^{fl/fl}$ (here referred as CKO) were considered to be controls. Genotyping of the animals was performed by PCR on genomic DNA from tail clippings using the following primers: *K14-cre_F*, 5′-accagagacggaaatccatcgctc-3′; *K14-cre_R*, 5′-tgccacgaccaagtgacagcaatg-3′; *Myc_F*, 5′-ccgaccgggtccgagtccctatt-3′; and *Myc_R*, 5′-gcccctgaattgctaggaagactg-3′. Presence of mutant mice in a typical litter of eight to 10 littermates followed a Mendelian distribution. All animal procedures were performed in accordance with the guidelines and approval of the Institutional Animal Care and Use Committee at the Icahn School of Medicine at Mount Sinai and the Johns Hopkins School of Medicine and adhered to the ARVO Statement for the Use of Animals in Ophthalmic and Vision Research.

Wound-Healing and Cell Proliferation

Corneal epithelial wound was induced as previously described.[27,28] Briefly, a corneal epithelial wound was induced in anesthetized mice using an Algerbrush (Ambler Surgical, Exton, PA, USA). To monitor wound size, fluorescein was applied to the wounded eye. After every procedure, eyes were treated with bacitracin antibiotic ointment (Fera Pharmaceuticals, Locust Valley, NY, USA). Eyes were photographed with a Leica L2 stereomicroscope (Leica Camera, Wetzlar, Germany) at 0, 24, 43, and 118 hours after wounding. Twenty-four hours after induction of the wound, mice were injected with a single intraperitoneal injection of 50 mg/kg of 5-bromo-2-deoxyuridine (BrdU; Sigma-Aldrich, St. Louis, MO, USA). Mice were sacrificed after 2 hours, and corneas were collected. After fixation for 40 minutes with 4% paraformaldehyde (PFA) in PBS, corneas were incubated in 2-N HCl at 37°C for 25 minutes, and the pH was adjusted to 7.4. Corneas were then immunolabeled using a rat anti-BrdU antibody (1:200, ab6326; Abcam, Cambridge, UK), flat-mounted in 4′,6-diamidino-2-phenylindole (DAPI)-complemented VectaShield (Vector Laboratories, Burlingame, CA, USA), and images were captured with a Zeiss LSM880 laser confocal microscope.

Histology and Immunostaining

For histological analysis, tissues were collected immediately after euthanasia by CO_2 asphyxiation, fixed overnight in 4% paraformaldehyde (PFA) in PBS, and embedded in paraffin. Hematoxylin and eosin (H&E) or hematoxylin staining was performed following standard procedures. For plastic sections, corneas were processed as previously described.[27,29] After embedding in Epon (Electron Microscopy Sciences, Hartfield, PA, USA), 1-µm semi-thin sections were cut with an ultramicrotome (Leica Ultracut UCT) and stained with methylene blue. The CE thickness was measured at the center of the cornea in five mice per group. For immunostaining, corneas were collected, fixed in 4% PFA in PBS for 20 minutes or 24 hours, and embedded in Tissue-Tek optimal cutting temperature compound (OCT; Sakura Finetek, Torrance, CA, USA) or in paraffin, respectively. OCT-embedded corneas were cryosectioned into 5-µm-thick sections that were hydrated and post-fixed for 5 minutes with 4% PFA in PBS at room temperature. After blocking with 2% BSA and 0.1% Triton X-100 in PBS for 1 hour, sections were incubated overnight with anti-Ki-67 (1:300, ab15580; Abcam), rabbit monoclonal anti-TP63 (1:100, M00167-1; Boster Bio, Pleasanton, CA, USA), or anti-ΔNp63 (1:200, ab735; Abcam) antibodies (Abs). After three 15-minute washes, sections were reacted with the appropriate Alexa Fluor 488 conjugated goat anti-rabbit (1:200, A-11034; Thermo Fisher Scientific, Waltham, MA, USA) or anti-mouse (1:200, A-11001; Thermo Fisher Scientific) Abs for 1 hour, washed three times for 15 minutes, and mounted with coverslips in DAPI-complemented mounting medium (VectaShield). Sections of paraffin-embedded tissue were deparaffinized or incubated in hot citrate buffer and immune-stained for Krt12 using rabbit polyclonal anti-K12

Investigative Ophthalmology & Visual Science

Abs at 2 µg/mL targeting either the N- or the C-terminus of the protein (a generous gift from Winston Kao, PhD, Department of Ophthalmology, University of Cincinnati, Cincinnati, OH, USA) as previously described.[30]

Confocal images were acquired with a Zeiss LSM800 or LSM880 confocal microscope. Quantification of the apical Krt12 signal was determined by measuring the length of the staining at the surface of the CE cross-sections using the "line" function in Fiji (ImageJ; National Institutes of Health, Bethesda, MD, USA).[31] Quantification of the Krt12 signal across the CE cross-sections was determined using the "plot profile" function in Fiji. For each cornea, 15 31-µm-wide line intensity profiles were recorded every 100 µm of a cornea cross-section length. The average intensity of each pixel was then plotted as a line graph rendering in Prism (GraphPad, San Diego, CA, USA) for each genotype. The signal intensity values for each genotype were normalized to the maximal intensity recorded. Quantification of the Ki67 and BrdU immunostaining was determined using the "cell count" function in Fiji. The TP63 and ΔNp63 immunofluorescence signals were recorded by acquiring confocal images using identical microscopy settings. Pixel intensity generated by a single fluorochrome was quantified using Fiji on original confocal images acquired using identical settings. The number of independent replicates, each comparing one CKO specimen versus a randomly selected control littermate, and the P values (Student's t-test; $^{*}P < 0.05$ and $^{**}P < 0.01$) are given in the figure legends. Student's two-tailed test was performed using Excel (Microsoft, Redmond, WA, USA).

Corneal Desquamation Assay by Dead Cell Labeling

Eyes were enucleated and incubated for 12 minutes in 0.4% trypan blue stain (Gibco Laboratories, Gaithersburg, MD, USA). Eyes were then fixed for 30 minutes with 3% glutaraldehyde, 1% PFA in 0.1-M sodium cacodylate buffer. Corneas were dissected, flat-mounted in PBS, and imaged with a Zeiss Axioplan 2 microscope.

Western Blot

Corneal epithelia were removed from the corneal surface using a dulled #15 scalpel, dissolved in 60 to 90 µL sample-loading buffer, boiled for 4 minutes, and centrifuged at 15,000*g* for 10 minutes. Equal volumes of supernatant were separated by 10% sodium dodecyl sulfate–polyacrylamide gel electrophoresis (SDS-PAGE) under reducing conditions and electro-transferred to a polyvinylidene difluoride membrane (EMD Millipore, Billerica, MA, USA). The membrane was blocked with 5% skim milk in PBS containing 0.1% Tween 20 and were then incubated at 4°C for 18 hours with 1:500 dilutions of primary Abs against Myc (1:1000, 13987, Cell Signaling Technology Danvers, MA, USA); phospho (p)-Ser62-Myc (1:200, 13748; Cell Signaling Technology); ΔNp63 (1:200, 619001; BioLegend, San Diego, CA, USA; ΔNp63 (1:200, 67825; Cell Signaling Technology); TAp63 (1:200, 938101; BioLegend); ETS1 (1:200, PA584591, Invitrogen, Waltham, MA); Notch1 (1:200, 14578581, Invitrogen, Carlsbad, CA, USA); Notch1 (1:200, 3608; Cell Signaling Technology); Krt14 (1:2000, MA511599; Invitrogen); or Krt12 (1:2000, PA567945; Invitrogen). After three washes, the membranes were incubated at room temperature for 1 hour with the appropriate goat anti-mouse or anti-rabbit horseradish peroxidase-conjugated secondary Abs (Thermo Fisher Scientific). Finally, the membranes were washed three times and protein bands were detected using enhanced chemiluminescence (ECL) reagent (Amersham Biosciences, Buckinghamshire, UK). All membranes were stripped and re-probed with a mouse monoclonal anti-glyceraldehyde 3-phosphate dehydrogenase (GAPDH) Ab (MA5-15738; Invitrogen) to provide a normalizing reference.

Real-Time Quantitative RT-PCR

Enucleated eyes were incubated overnight in 5 mg/mL Dispase (Invitrogen) in Dulbecco's Modified Eagle Medium/Nutrient Mixture F-12 (DMEM/F-12) and HEPES (Gibco) at 4°C. The CE was peeled off and total RNA was isolated using the RNeasy Micro Kit (Qiagen, Hilden, Germany) according to the manufacturer's instructions. RNA was reverse transcribed from 100 µg of total RNA using Invitrogen SuperScript III Reverse Transcriptase and oligo(dT) primers as previously described.[27,29] RT-PCR was performed using a mix of cDNA, SYBR Green reagent (Qiagen), and 10 µM of primers. The sequences of primers for *p63* isoforms were selected using Primer3 Output program technology (Massachusetts Institute of Technology, Cambridge, MA, USA) and were as follows: ΔNp63 forward, 5′-GGAAAACAATGCCCAGACTCA-3′; ΔNp63 reverse, 5′-GTCACGCTATTCTGTGCGTG-3′; TAp63 forward, 5′-CACCCAGACAAGCGAGTTCCT-3′; TAp63 reverse, 5′-CACTGAGGTCTGAGTCTTGCAT-3′; p63α forward, 5′-TCCGACATGCCATCTGGAAG-3′; p63α reverse, 5′-GCATCGATCACACGTTCACC-3′; p63β forward, 5′-TGGCTGGAGACATGAATGGAC-3′; and p63β reverse, 5′-CAGACTTGCCAAATCC. These primers were designed from the reference sequences in the GenBank database, accession numbers AF075439 (ΔNp63α), AF075436 (TAp63α), and AF075435 (TAp63β). Primers for Ets1, Notch1, and Gapdh have been previously published and were as follows: Ets1 forward, 5′-CCCTGGGTAAAGAATGCTTCC-3′; Ets1 reverse, 5′-GCTGATGAAGTAATCCGAGGTG-3′[32]; Notch1 forward, 5′-AGTGTGACCCAGACCTTGTGA-3′; Notch1 reverse, 5′-AGTGGCTGGAAAGGGACTTG-3′[33]; Hey1 forward, 5′-GCTGAGATCTTGCAGATGAC-3′; Hey1 reverse, 5′-CAACTTCGGCCAGGCATTCC-3′; Hes1 forward, 5′-GTCAACACGACACCGGACAA-3′; Hes-1 reverse, 5′-CCTTCGCCTCTTCTCCATGA-3′; Maml1 forward, 5′-GCACAGCGCGGTCATGGAGC-3′; Maml1 reverse, 5′-GCGCTTGGCCTTGGCCTGGA-3′[27]; Gapdh forward, 5′-AGGTCGGTGTGAACGGATTTG-3′; and Gapdh reverse, 5′-GGGGTCGTTGATGGCAACA-3′.[34] The reactions were carried out in an ABI PRISM 7900HT Sequence Detection System (Applied Biosystems, Foster City, CA, USA) using a PCR program consisting of 40 cycles of 95°C for 15 seconds, 55°C for 15 seconds, and 72°C for 30 seconds. Data were analyzed using the $2^{-\Delta\Delta Ct}$ method, with *Gapdh* transcript as a reference.

Statistical analysis and quantification

Data were statistically analyzed using the Student's t-tests from at least three independent experiments using Microsoft Excel 2017. Error bars represent mean ± SD. $P < 0.05$ was considered significant.

Investigative Ophthalmology & Visual Science

Results

The CKO Mouse Displays Postnatal Growth Delay and Maturation Abnormalities in Multiple Stratified Epithelia

In order to ablate *Myc* in ectoderm-derived stratified epithelia, we crossed mice with floxed *Myc* allele ($Myc^{fl/fl}$)[25] with the *Tg(KRT14-cre)1Amc/J* (*K14-cre*) transgenic line[26] in which the Cre expression is driven by the promoter of the *Krt14* gene to obtain the mutant mouse line *K14-cre;*$Myc^{fl/fl}$ (hereafter referred to as CKO). The $Myc^{fl/fl}$ and *K14-cre* alleles were maintained on FVB and mixed C57BL/6 and 129 genetic backgrounds, respectively. Thus, littermates had a mixed background, resulting in white, brown, or black coat color. White coat mice persisted throughout generation F5. The phenotypes presented in this study remained consistent in CKO mice of the 52 litters generated for this study covering a total of seven generations. However, white-coat CKO mice obtained in F2 and F3 displayed a more severe phenotype with regard to the lower lip and the eyelid when compared with CKO mice with a darker coat (Figs. 1, 2); no differences in severity and/or penetrance were detected for the phenotypes affecting the tail, coat pattern, and ocular surface in mutants of any coat color from any generation (Fig. 1). Moreover, no differences in severity and/or penetrance were observed for the phenotypes between male and female mice, so both sexes were included in this study.

At birth, the overall external morphology and the body weight of the CKO mice appeared indistinguishable from those of the control littermates, including *K14-cre*, *K14-cre;*$Myc^{fl/+}$, $Myc^{fl/+}$, and $Myc^{fl/fl}$ genotypes (Fig. 1A). However, starting from postnatal day 7 (P7), the weight of the CKO mice increased at rates that were ~50% lower than those displayed by the control littermates (Figs. 1A, 1B). Additionally, mutant mice exhibited abnormalities of the epidermis and other ectodermal-derived epithelia. The organized arrangement of the body hair and the periodicity of the pigmentation observed in the control were both disrupted in the mutant (see insets in Figs. 1Bi–1Biv). Most of the CKO mice obtained for this study developed exudating abrasions in the skin of the tail between P30 and P40 (Fig. 1B). Such abrasions were not observed in any control littermates. A consistent and striking abnormality in CKO mice was a visible degeneration of the lips; in particular, the lower lip of the CKO mice was largely receded and translucent and frequently displayed a blood exudate (Fig. 1C). In CKO mice with a white coat, which in mixed-background mice is an indication of abundant albino FVB genetic background,[35] the gross lip degeneration was more extensive, with overt degeneration extending to the upper lip (Fig. 1C). These defects were not apparent at birth; rather, they developed and became more pronounced during postnatal development and growth. The CKO mice died spontaneously between 6 and 8 weeks of age, thereby limiting experimentation in adult animals.

To further assess the nature of epithelial abnormalities caused by the absence of Myc we analyzed histological sections of the tail, mouth, and ocular surface of CKO and control mice. In the tail, the epidermis of the CKO mouse displayed an abnormally abundant pattern of exfoliation of the cornified layers (Fig. 1D, top frames). The macroscopic tail abrasion observed in the mutant showed in Figure 1B was underpinned by a loss of epidermal continuity (Fig. 1D, bottom frame, arrows).

To track the lip degeneration we first examined neonatal (P2) heads (Fig. 1E, top frames). At this stage, the mucocutaneous epithelium of the control and CKO littermates appeared indistinguishable. In contrast, after 7 weeks, the lip zone of the CKO mouse displayed a thin, undersized mucocutaneous epithelium loosely attached to the underlying dermis, whereas in the control specimen this area of the lip was characterized by a heavily layered and cornified epithelium (Fig. 1E, middle frames and insets). The bottom frames in Figure 1E show two examples of the transition between the intact skin and heavily abraded lip zones. For these images, because the acquired cellular complexity of the exposed dermis hindered epithelial visualization under transmitted light, H&E staining was visualized by epifluorescent illumination using an Alexa Fluor 488 filter set.

Thus, *Myc* ablation in Krt14-expressing tissues appears to play an essential role in epithelial stratification/maturation. These findings are consistent with previous studies where *Myc* was ablated in Krt5-expressing epithelia.[17] These results also suggest that the severity of a specific phenotype such as abrasion of the lip can vary as a possible function of a specific genetic background.

The Absence of Myc Leads to Abnormal CE Stratification

To further investigate the nature of the stratification/maturation phenotype described above in complex epithelia, we focused on the CE. In addition to being a lining of critical importance for vision, the CE provides unique advantages for the study of the effects of gene expression perturbation on the homeostasis and repair of stratified epithelia. First, the CE is easily accessible for physical manipulation, and second, it presents a relatively simple architecture and growth and differentiation dynamics, occasionally referred to as the X, Y, Z model.[22] Overt differentiation along the basal cells is linked to the transition of migrating cells from the limbus, where stem cells reside, to the avascular corneas. At a steady state, the supply of progeny from SCs, the centripetal migration, and upward movement (stratification) of the latter are designed to match the rate of cell exfoliation at the surface of the cornea. The four to six cell layers of stratification can be partitioned into three cell zones according to cell morphology: the basal layer with cuboidal cells, the early suprabasal layers with wing-shaped cells, and the late or upper squamous layers composed of flat cells that are approaching the stage of devitalization and desquamation.

Western blot analysis of isolated CE revealed that Myc was expressed in the CE of wild-type mice but was undetectable in the CE of CKO mice, confirming the efficiency of tissue-specific Myc ablation in our mutant (Fig. 2A). Cross-sections of paraffin-processed corneas stained with H&E and hematoxylin only (Figs. 2B, 2C) revealed a thicker CE in the mutant than in the control. Specifically, we found that, in the CE of the mutant, the number of suprabasal cell layers was higher than that found in the CE of the control (Figs. 2B, 2C). In contrast, at the limbus, where the mouse epithelium consists of only one or two layers of undifferentiated cells, there were no detectable differences between mutant and control mice (Fig. 2D). These observations suggest a delay in the transition from basal/suprabasal cell layers to flattened cells during epithelial maturation.

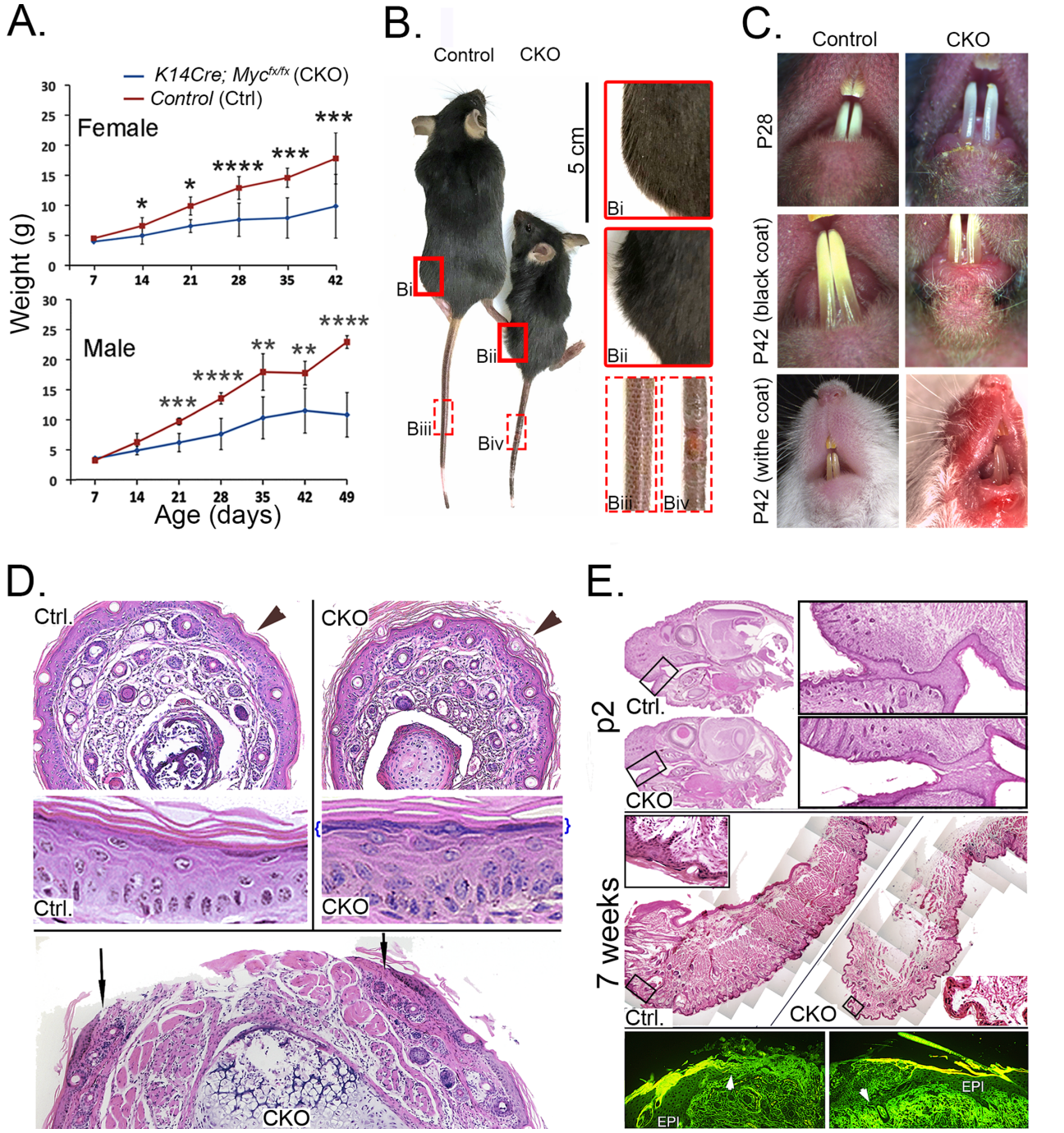

Figure 1. Main phenotypic manifestations of the *K14-cre;Myc*$^{fl/fl}$ mouse. (**A**) Weight gain for male and female *K14Cre;Myc*$^{fl/fl}$ versus control littermates (mean ± SD; $n = 4$ CKO females, 8 control females, 4 CKO males, and 6 control males). (**B**) Dorsal view of 7-week-old CKO and control littermates. *Insets* **Bi** and **Bii** show disorganization of the hair pattern; *insets* **Biii** and **Biv** show a loss of pigmentation periodicity and spontaneous development of abrasions in the tail. (**C**) Lip degeneration in black and white mixed-background CKO mice. Pronounced abrasions at the mucocutaneous junctions develop in 100% of these CKO mice by the second or third week of life. The extent of the abrasions is more pronounced in white-background CKO mice, where it extends to the upper lip (bottom micrographs). (**D**) Histological defects in the tail of adult mice. (*Top frames*) The desquamation pattern observed in cross-sections of the tail in the epidermis (*arrowheads*) of the CKO is markedly more abundant than the one observed in the control. (*Bottom frame*) A histological section at the intersection between the epithelialized and abraded area of the tail in the CKO mouse. *Arrows* point to the epidermal ends of the abrasion. (**E**, *top frames*) neonatal mice heads. There are no evident overt differences in mucocutaneous epithelia between the CKO and control mice. (*Center frames*) The CKO epithelium is only one or two layers thick, and the Krt layer is very thin compared with that of the control (see *insets*). (*Bottom frames*) Skin side of the mucocutaneous zone; epifluorescent visualization of H&E staining. *Arrowheads* indicate desquamation areas. *Arrows* point to the epidermal ends of the tail abrasion shown in **Biv**. EPI, epithelium; ns, not significant ($P \geq 0.05$, Student's *t*-test). *$P < 0.05$, **$P < 0.001$, ***$P < 0.0001$, ****$P < 0.00001$. *Scale bars*: 500 µm.

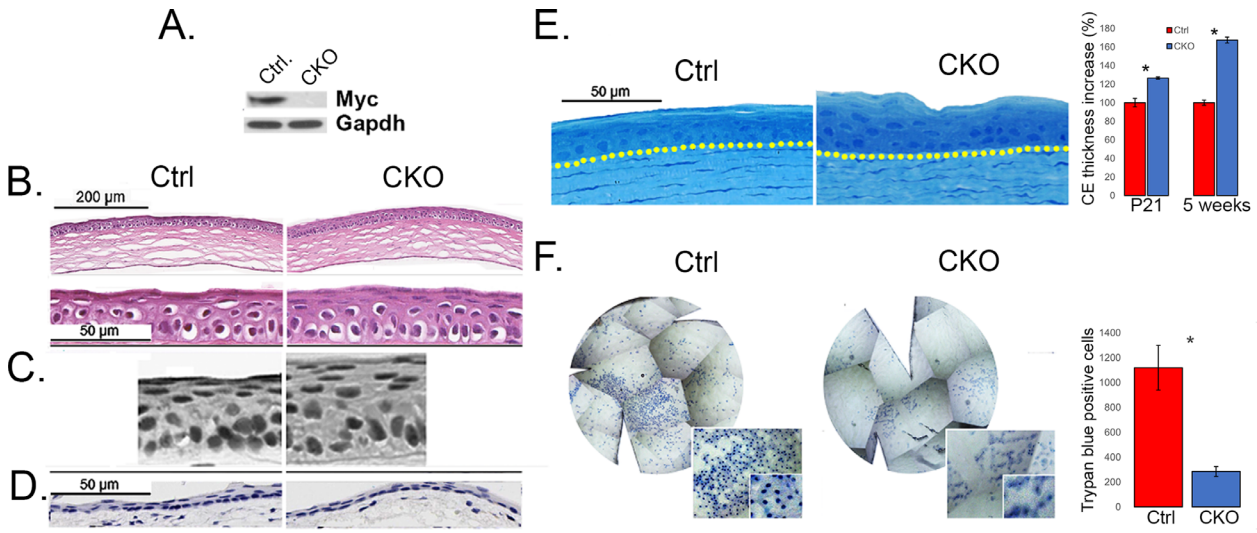

Figure 2. Ablation of *Myc* results in abnormal CE thickness and strata organization. (**A**) Myc western blot of isolated CE from control and CKO mice corneas. (**B–D**) Hematoxylin-only staining of cross-sections of central corneas (**B**, **C**) and the limbus (**D**) from mice at P21. (**E**) Semi-thin cross-sections of corneas embedded in epoxy resin from mice at P21. Representative micrographs (*left*) and mean central CE thickness (*right side*) are shown (mean ± SD, $n = 3$). (**A–E**) Images show that, in the CKO mice, the normal flattening of the cells at the surface of the CE was delayed, generating thicker strata incorporating extra superficial nucleated layers. (**F**) Representative micrographs of the corneal surface of P55 mice following whole eye exposure to 0.4% trypan blue in PBS for 5 minutes. In the CKO corneas, the frequency of staining profiles corresponding to overtly devitalized cells is less than 1/5 of the frequency of control corneas (mean ± SD, $n = 3$/group). ns, not significant ($P \geq 0.05$, Student's *t*-test). *$P < 0.05$, **$P < 0.001$.

To confirm the differences in stratification observed by H&E staining, we obtained plastic sections from glutaraldehyde-fixed corneas. This approach allows preserving tissue architecture and dimensions close to the in vivo tissue condition.[27] Plastic cross-sections show that the average thickness of the whole CE of the mutant was 30% higher than that of the control (Fig. 2E). At the cellular level, the main morphological difference in the CE stratification of the mutant appeared to originate from a reduction of the normal flattening of the maturing stratifying cells as they approached the surface position (Fig. 2E). Next, we further investigated the possibility that morphological differences between mutant and control CE of cells near the surface may translate into differences in the desquamation process. Timely maturation and desquamation are critical for the maintenance of an uninterrupted epithelial surface that is refractory to pathogen attachment, stabilizes the tear film, and presents a high resistance to passive fluid infiltration.[36] Cell removal from the cornea surface also induces Z0-1 synthesis and stratal distribution.[37]

Because devitalization of cells at the CE surface precedes desquamation, we have determined the number of fully devitalized surface cells in CKO and control mice using trypan blue surface staining in live CE as described in Methods and in Sokol et al.[38] The corneal surface of the control contained a substantial number of well-defined stained nuclei. In contrast, staining of the CKO cornea under identical conditions generated a fuzzy and weak stain profile of superficial cells (Fig. 2F). Moreover, the number of superficial cells with stained nuclei detected in control corneas was at least three times larger than the number detected in the mutant (Fig. 2F). The difference in surface staining could reflect a perturbation in the rate of surface cell devitalization or the rate of exfoliation of the devitalized cells. Taken together, these findings suggest that the perturbation in stratal dynamics in the mutant may extend to affect the phenotype of the surface cells and affect rates of CE desquamation.

Myc Deficiency Delays CE Repair and Impairs Wound-Healing–Induced Hyperproliferation But Not Proliferation Rates at Homeostasis

Because CKO mice display an increase in CE thickness we investigated the role of Myc in CE proliferation. We examined rates of cell division and Myc expression in the CE at homeostasis and during repair in both mutant and control mice. In control littermates, a nominal limbus-to-limbus (1.5-mm diameter) Algerbrush-generated debridement closed in approximately 24 hours; in contrast, in the CKO, a similar circular wound was reduced by only 40% after 24 hours and did not completely close even 5 days after wounding (Fig. 3A). Proliferation rates were assessed by monitoring BrdU incorporation in flat corneal mounts of mice injected 2 hours prior to the analysis.[27]

Consistent with the differences in CE wound closure, the proliferation rates of CE basal cells, assessed by counting BrdU+ versus BrdU– nuclei 24 hours post-wounding, underwent a threefold increase (from 7% to 21%) in the control but only a twofold increase (from 6% to 13%) in the CKO. Thus, the increase of proliferation rates induced by wounding in the CE of the CKO mice was half that of the control mice (Fig. 3B). In contrast, at homeostasis, proliferation rates detected in the mutant CE were indistinguishable from those of the control. This latest result was also confirmed in corneal cross-cryosections of both CKO and control mice by staining of Ki-67, a nuclear marker for cell proliferation, at CE steady state (Fig. 3C).

To relate the differential impact of *Myc* ablation on the homeostatic and wound response conditions, we examined

Investigative Ophthalmology & Visual Science

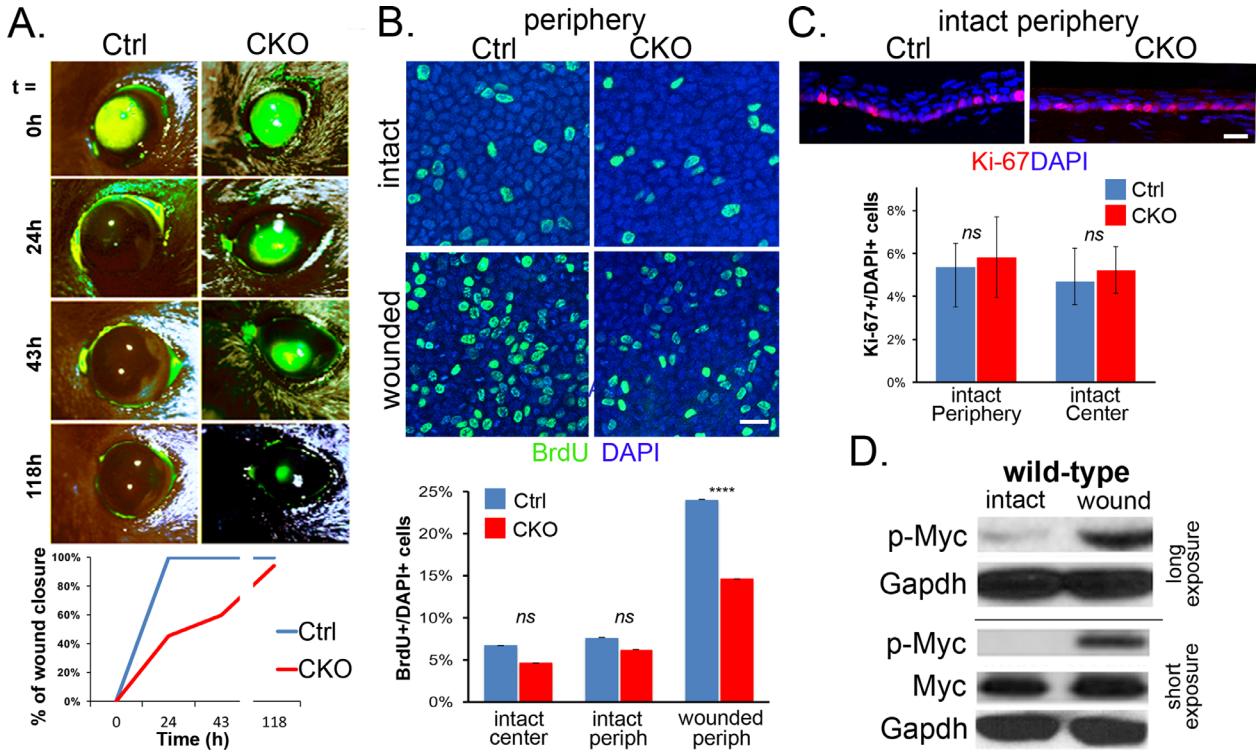

Figure 3. CE wound-healing response in the absence of Myc. (**A**) Wound closure of the CE in 2-month-old mice of a circular Algerbrush-generated corneal debridement with a diameter of 1.5 mm. The wound size was visualized by fluorescein staining, and rates of wound closure were quantified over time as indicated ($n = 3$/group). (**B**) Representative images of stained flatmounts showing BrdU (*green*) incorporation at the corneal periphery in intact corneas or 24 hours after debridement (wounded). The proliferation rate was determined by normalizing the number of BrdU-positive nuclei to the total number of DAPI-stained nuclei (mean ± SD, $n = 2$/group). (**C**) Ki-67 staining of cross cryosections at the periphery of intact corneas. The ratio between stained basal cells expressing Ki67 (*red*) and DAPI-stained nuclei (*blue*) was quantified. Note that in the intact CE there were no differences in the Ki67 stain and BrdU incorporation rates between control and CKO littermates (mean ± SD, $n = 3$/group). (**D**) Western blots for Myc and p-(Ser62)-Myc (pMyc) in isolated CE before and 24 hours after 1.5-mm-diameter corneal debridement relative to two similar experiments**.** Note that, before debridement, the activated Myc, p-(Ser62)-Myc, levels were not detectable in one experiment (lower panels) but were faintly visible in another (higher panels). ns, not significant ($P \geq 0.05$, Student's *t*-test). *$P < 0.05$, **$P < 0.001$, ***$P < 0.0001$, ****$P < 0.00001$. *Scale bars*: 25 µm.

the status of Myc protein in intact and wounded wild-type mice CE. Myc activity depends on its activation by phosphorylation on Ser62. Western blots against this epitope in intact CE yielded an extremely faint signal in two independent samples (Fig. 3D). This suggests that only a very small fraction of the total Myc appears to be phosphorylated and thus active in the intact tissue. In contrast, during wound healing, the amount of p-(Ser62)-Myc was markedly elevated in wild-type CE collected 24 hours after wounding, whereas the total amount of the Myc protein remained unchanged or underwent only a minimal increase (Fig. 3D). Thus, p-(Ser62)-Myc levels undergo a significant increase during wound healing and are positively correlated with the occurrence of wound-healing–induced hyperproliferation.

Myc Ablation Modifies Krt12 Stratal Distribution and Enhances ΔNp63, ETS1, and Components of the Notch Signaling Pathway

The phenotypic abnormalities observed in the stratified epithelia of the CKO mice suggest an inability to undergo timely differentiation steps associated with stratal maturation. Thus, we examined the spatial expression of Krt12, the corneal-specific cytokeratin associated with CE differentiation (Fig. 4A). Immunofluorescence labeling of cross-sections of paraffin-embedded corneas from CKO and control mice with two distinct anti-Krt12 antibodies revealed no differences in intensity and distribution of Krt12 at the basal cell layer (Fig. 4A). In contrast, flat Krt12 high-intensity staining superficial cells covered ~50% of the CE outer surface in the CKO but only ~10% of the control CE. A possible explanation of this CKO feature is that the coordination of cellular maturation, devitalization, and exfoliation is delayed or perturbed in the CKO, resulting in longer permanence of surface cells in a vital state, as already suggested by the reduction of trypan blue surface staining (Fig. 2F).

Given the overt differences in the patterns of stratal maturation, we examined the levels of gene and protein expression of three factors that have been associated with changes in stratified epithelial differentiation. The *TP63* gene, which generates transactivating (TAp63) and N-terminally truncated transcripts (ΔNp63), in its various isoforms is involved in all stages of epithelial development, preservation of proliferative capacity, and differentiation of the CE.[39,40] ETS1 has been shown to delay epidermal differentiation.[41] In contrast, Notch1 acts as a differentiation inducer in both the epidermis and the CE[42] and has been reported to be repressed by ETS1[33] and by the epithelial-specific ΔNp63 isoform.[43]

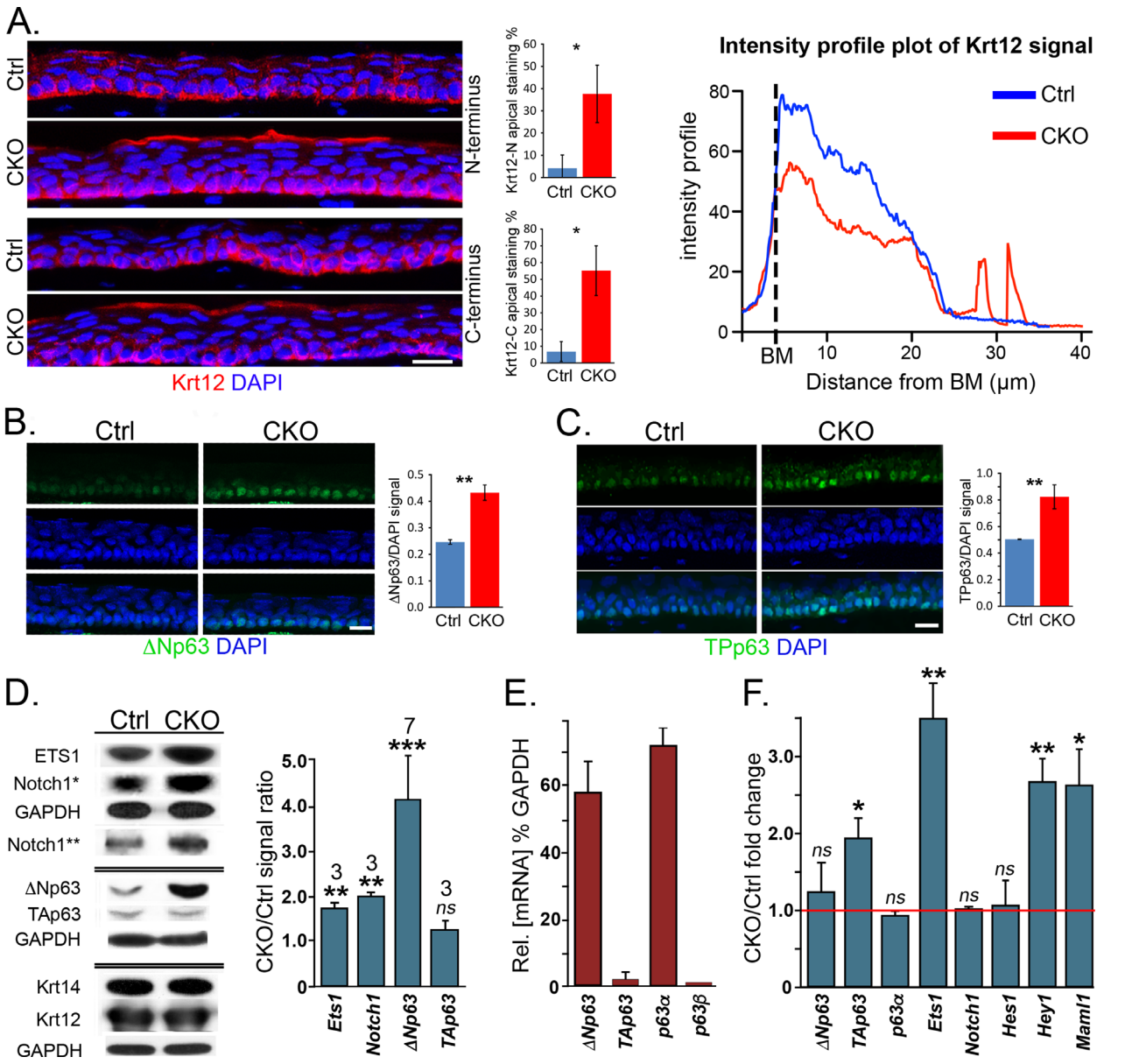

Figure 4. Expression and localization of TP63 isoforms and other selected factors associated with CE homeostasis and stratification in absence of *Myc*. (**A**, *left panel*) CE immunostaining of Krt12 (*red*) and DAPI (*blue*) on cross-sections of the paraffin-embedded cornea. The Abs utilized were directed to either the N- or the C-terminus of the Krt12 protein. Krt12 accumulation at the CE surface observed in the mutant using either Ab was severely reduced in the CE of the CKO. *Bar graphs* represent the percentage of Krt12 apical staining along the CE length of cornea cross-sections (mean ± SD, $n = 3$). (**A**, *right panel*) Line-intensity profile plot of Krt12 fluorescence signal across a CE cross-section. The *y*-axis represents the average intensity of 15 line-intensity scans (31 μm wide) from the basal membrane (BM) to the apical side of the CE taken every 100 μm along the length of each cornea section. The *x*-axis represents the length of the line scan from the BM to the apical side of the CE ($n = 3$). (**B**) CE immunostaining with Ab directed to the epithelial-specific ΔNp63 ($n = 4$/group). (**C**) CE immunostaining with the pan (TP) p63 Abs ($n = 2$ control and 4 CKO). The *bar graphs* in **B** and **C** describe the mean ± SD values of p63 intensities (*green fluorescence*) over the whole epithelium, normalized by the corresponding nuclear stain (*blue fluorescence*). (**D**, *left panel*) GAPDH-normalized CKO/control chemiluminescence signal ratios (mean ± SD). Number of independent replicates for each protein are indicated on top of the bars. *Myc* ablation led to a fourfold increase of ΔNp63 and about twofold increases in ETS1 and Notch 1. Krt14 and Krt 12 displayed no substantial differences in two duplicates and were not quantitated. (**E**) Level of expression of p63 isoforms relative to *Gapdh* in the wild-type mouse (mean ± SD, $n = 3$/group). (**F**) Expression of p63 isoforms and genes involved in the CE differentiation. Data are represented as the fold change in the CKO relative to the control ($n = 3$/group). ns, not significant ($P \geq 0.05$, Student's *t*-test). *$P < 0.05$, **$P < 0.001$. *Scale bars*: 25 μm.

Immunostaining of corneal cross cryosections with an antibody directed to ΔNp63 stained the basal CE cells in both mutant and control samples, but the fluorescence signal in the mutant was about two times more intense than the one detected in the control (Fig. 4B). A similar result was obtained by using a pan-anti-TP63 Ab recognizing all TP63 isoforms, including the ΔNp63 isoform (Fig. 4C). We could not obtain a reliable and specific immunofluorescent signal for the TAp63 isoform using commercially available Abs. Protein levels were determined by western blot

and immunostaining. Representative results of immunoblots and means ± SDs of the CKO/control expression ratios are shown in Figure 4D. Compared with the control, the CE of the mutant displayed protein levels of Ets1, Notch1, and ΔNp63 that were higher by 1.8-, 2.0-, and 4.1-fold, respectively (Fig. 4D). In contrast, levels of the TAp63 protein remained unchanged. Additionally, it is pertinent to mention that the film exposure time required to generate a band for TAp63 of an intensity similar to that of the ΔNp63 band was about 20 times longer, suggesting that TAp63 is only a minor component of the total amount of TP63 (Fig. 4D). Finally, despite the differences in strata distribution (Fig. 4A), Krt14 and Krt12 protein levels of the mutant CE were indistinguishable from those of the control (Fig. 4D).

To further assess the expression of TP63 isoforms and other genes associated with CE differentiation, we measured variations of their mRNA levels by RT-qPCR (Figs. 4E, 4F). In wild-type CE, the mRNA levels of Δ*Np63* were approximately 20 times higher than those of *TAp63* (Fig. 4E). Moreover, and as shown for the human CE,[44] the *α* isoform was largely the predominant C-termini isoform of TP63 (Fig. 4E).[45] Despite the remarkable increase seen in the western blots, there was no change in the level of Δ*Np63* mRNA between the mutant and the control CE (Fig. 4F). Consistent with the increase of ETS1 protein levels, we detected a threefold increase in *Ets1* mRNA in the CKO compared with the control (Fig. 4F). Finally, contrary to the increase of the Notch1 protein in the mutant, the amount of *Notch1* mRNA remained unchanged between mutant and control CE (Fig. 4F). Finally, we detected a twofold increase in the mRNA of two Notch target genes, *Hey1* and *Maml1*, in the mutant CE compared with control (Fig. 4F). Thus, taken together, our results show that the absence of Myc in the CE leads to defective localization and expression of several markers involved in maintaining the normal CE architecture at homeostasis.

Discussion

Our results indicate that the ablation of *Myc* in Krt14-expressing epithelial linings leads to disturbances of multiple stratified epithelia. The mucocutaneous junction of the lip and the epidermis of the tail display a reduction in the thickness of the protective cross-linked cytokeratin (keratinized) layer. This decreased protection may, in conjunction with mechanical stress or physical friction, lead to the observed tail and lip abrasions. The latter may have a critical effect on animal survival. The reduced weight gain in CKO mice starts by the second week of life and could be the result of an inability of the pups to initially compete for their mother's milk. Mucocutaneous abrasion could also hinder the consumption of solid food later on. In any event, the premature death of all CKO mice, whether as a result of malnutrition or other causes, placed a time limit of 7 weeks on our study. Overall, these changes in keratinization suggest that the main effect of *Myc* ablation in the keratinizing epithelia is to delay the final stages of cell maturation.

The epidermal features found in our CKO mice appear consistent with those previously reported for *Krt5Cre;Myc*$^{flox/flox}$ mice.[17] In this mutant, the skin also developed postnatal abrasions. However, the severe lip abrasions, the reduced growth rates, and the premature death displayed by our CKO mice were not reported for the *Krt5Cre;Myc*$^{flox/flox}$ mouse. The differences between the two mutants could likely be attributed to a well-documented effect of genetic background on the penetrance of a given phenotype.[46–48] The differential impact of *Myc* ablation on lip lesions of brown and white coat mutants is consistent with this possibility; however, the de novo expression of Krt5 and Krt14 in the different ectoderm-derived epithelia may also play a role in generating phenotypic differences.[49]

The nature of the abnormalities detected in the skin prompted us to investigate the function of Myc in the context of CE differentiation, renewal, and repair. In the CE, *Myc* ablation caused no detectable effect on the proliferation of basal cells at rest. This result is consistent with the presence of very low levels of the active form of Myc, p-(Ser62)-Myc, in the CE at homeostasis (Fig. 3D). In contrast, we detected high levels of activated Myc during wound healing and found that the rates of wound closure were significantly reduced in the absence of Myc. Thus, phosphorylated Myc appears unlikely to play any substantial role in the slow proliferation existing under the rest state. Nevertheless, subtle, difficult-to-detect localized changes in Myc phosphorylation may be critical for coordination between the rates of surface cell sloughing and basal proliferation that ensure the constancy of the stratal thickness at homeostasis. On the other hand, elevated levels of p-(Ser62) during wound healing are consistent with the critical role of Myc for the activation of hyperproliferation and hence the strong effect of *Myc* ablation on the wound closure rate. A role of Myc in the migration rate of basal cells is also plausible and remains to be examined.

At steady state, effects of *Myc* ablation were observed solely at the apex of the stratum. At the histological level, the normal flattening of cells during their migration toward the corneal surface was less pronounced in the mutant CE and exfoliation appeared to be delayed, resulting in a thicker epithelium. A retardation of the spontaneous devitalization process was suggested by the reduction in the percent of surface cells showing distinct trypan blue staining.[37,50] Based on the differences in patterns of Krt12 staining at the surface, the delay seemed to result in the retention of vital cells at the surface, which under normal *Myc* expression undergo timely devitalization. In summary, *Myc* ablation seems to delay CE terminal differentiation, which is consistent with findings relative to the opposite scenario showing that *Myc* overexpression in keratinocyte accelerates epidermal differentiation.[9]

Using western blot and RT-qPCR, we were able to identify perturbances in the expression of three proteins prospectively associated with CE or epidermis differentiation: p63, EST1, and Notch1. Regarding p63, the measurements indicated that (1) as in humans, the predominant isoform found in the CE is ΔNp63*α*[51]; (2) Myc ablation caused a dramatic increase of ΔNp63 levels at steady-state; (3) the increase in ΔNp63 protein levels reflected increased p63 in a substantial fraction of the total basal cell nuclei; and (4) this increase does not derive from an increase in Δ*Np63* gene expression. Thus, the absence of Myc could favor the stabilization of synthesized ΔNp63. This truncated form of p63 is essential for maintenance of the proliferative capacity of the precursor cells in multiple ectodermal derived cells.[52] In the human CE, high expression levels of ΔNp63 have been reported to be associated with the less differentiated state of the basal cells at the limbus.[51,53,54] Thus, the high accumulation of this isoform may directly or indirectly cause a slowing of earlier differentiation that leads, ultimately, to decompensation of final maturation stages. To our knowledge, this is the first report of an effect of Myc on the levels of this critical regulator of epithelial cell survival and proliferative

Investigative Ophthalmology & Visual Science

potential. The near absence of activated Myc at homeostasis of an intact epithelium presents a challenge in trying to establish a link among *Myc* ablation, changes in differentiation, and enhanced p63 stability. It is possible that at rest a brief Myc activation takes place, resulting in minimal levels detected by western blot. Alternatively, unphosphorylated Myc may exert an effect through its ability to bind to numerous partners.[55]

The increase of *Ets1* transcript and protein levels detected in the mutant as a consequence of *Myc* ablation is consistent with the reported delay of terminal epidermal differentiation in mice overexpressing *Ets1*.[33] Our results also show that Myc deficiency leads to an accumulation, although modest, of Notch1 in the CE of the CKO mouse; however, given that Notch1 is associated with the stratified layers, the increase of Notch1 protein could be due to an increase in the suprabasal cell mass. In support of this possibility, the levels of the Notch1 transcript found in the CE of the mutant were indistinguishable from those of the control. Moreover, we found that the expression of target genes of the Notch signaling pathways, including *Hey1* and *Maml1* but not *Hes1*, is elevated in Myc-deficient CE. In the CE, Notch has been shown to play a critical role in cell differentiation, maintenance of the epithelial barrier, and cell fate determination of limbal stem cells.[56–59] Importantly, although constitutive activation of the Notch pathway by transgenic expression of the active *Notch1* intracellular domain (NICD) in the mouse CE or by recombinant Jagged1, leads to the upregulation of *Notch1*, *Hes1*, and other Notch target genes, it does not appear to alter cell proliferation and differentiation nor the overall morphogenesis and strata organization of the CE at homeostasis in vivo and in vitro.[60,61] This observation strongly supports the possibility that the morphological defects of the CE observed at homeostasis in the absence of Myc are not resulting from the upregulation of a subset of Notch target genes including *Hey1* and *Maml1* nor by the increase of the Notch1 protein levels. On the other hand, overexpression of NICD promotes and accelerates CE wound closure, possibly due to a more rapid wound-induced early proliferation response.[61] In contrast, in this study, we found that the absence of Myc delayed wound closure, probably because Myc during wound-induced proliferation response acts upstream of Notch.

Given the phenotype and protein disturbances observed in the CE, it will be intriguing to examine whether they also occur in other stratified epithelia. On *para-* or fully keratinized tissues, late-stage differentiation involves the formation of a hardy cross-linked envelope. Failure to fully develop such a protective layer may be enough to allow development of the devastating breaks in the oral mucosa observed in the CKO mouse. In conclusion, we have uncovered a dual role of Myc in maintaining the normal thickness and architecture of murine CE at homeostasis and promoting basal cells hyperproliferation during CE repair. The causative relationships or interplay among the three proteins that undergo expression changes as a result of Myc ablation (ΔNp63, Notch1, and Est1) require further analysis, possibly using a well-established in vitro cellular system.[62]

Acknowledgments

The authors thank Qing Liu for the excellent technical assistance, Varuni Rastogi for her help with quantitative analysis, and the members of the Wilmer Cornea Group for their helpful input and discussions. We are particularly grateful to James Foster for his help with data rendering and critical comments on the manuscript.

Supported by grants from the National Eye Institute, National Institutes of Health (EY030661 to CI, EY 030567 and EY029279 to JMW, DK126450 to DKS); by a core grant to the Wilmer Eye Institute (EY001765); by a Challenge Grant from Research to Prevent Blindness (RPB) to JMW; by a grant from New York Eye and Ear Infirmary to JMW; by a grant from the Eisinger Family; by a Wilmer Eye Institute Seed Fund to CI; and by an unrestricted grant from RPB to the Wilmer Eye Institute.

Disclosure: **C. Portal**, None; **Z. Wang**, None; **D.K. Scott**, None; **J.M. Wolosin**, None; **C. Iomini** None

References

1. Marques-Pereira JP, Leblond CP. Mitosis and differentiation in the stratified squamous epithelium of the rat esophagus. *Am J Anat*. 1965;117:73–87.
2. Rheinwald JG, Green H. Serial cultivation of strains of human epidermal keratinocytes: the formation of keratinizing colonies from single cells. *Cell*. 1975;6(3):331–343.
3. Lavker RM, Sun TT. Epithelial stem cells: the eye provides a vision. *Eye (Lond)*. 2003;17(8):937–942.
4. Mackenzie IC, Bickenbach JR. Label-retaining keratinocytes and Langerhans cells in mouse epithelia. *Cell Tissue Res*. 1985;242(3):551–556.
5. Lehrer MS, Sun TT, Lavker RM. Strategies of epithelial repair: modulation of stem cell and transit amplifying cell proliferation. *J Cell Sci*. 1998;111(pt 1):2867–2875.
6. Merzel J, Leblond CP. Origin and renewal of goblet cells in the epithelium of the mouse small intestine. *Am J Anat*. 1969;124(3):281–305.
7. van der Flier LG, Clevers H. Stem cells, self-renewal, and differentiation in the intestinal epithelium. *Annu Rev Physiol*. 2009;71:241–260.
8. Morrison SJ, Weissman IL. The long-term repopulating subset of hematopoietic stem cells is deterministic and isolatable by phenotype. *Immunity*. 1994;1(8):661–673.
9. Arnold I, Watt FM. c-Myc activation in transgenic mouse epidermis results in mobilization of stem cells and differentiation of their progeny. *Curr Biol*. 2001;11(8):558–568.
10. Bull JJ, Pelengaris S, Hendrix S, Chronnell CMT, Khan M, Philpott MP. Ectopic expression of c-Myc in the skin affects the hair growth cycle and causes an enlargement of the sebaceous gland. *Br J Dermatol*. 2005;152(6):1125–1133.
11. Waikel RL, Kawachi Y, Waikel PA, Wang XJ, Roop DR. Deregulated expression of c-Myc depletes epidermal stem cells. *Nat Genet*. 2001;28(2):165–168.
12. Wilson A, Murphy MJ, Oskarsson T, et al. c-Myc controls the balance between hematopoietic stem cell self-renewal and differentiation. *Genes Dev*. 2004;18(22):2747–2763.
13. Delgado MD, Leon J. Myc roles in hematopoiesis and leukemia. *Genes Cancer*. 2010;1(6):605–616.
14. Watt FM, Frye M, Benitah SA. MYC in mammalian epidermis: how can an oncogene stimulate differentiation? *Nat Rev Cancer*. 2008;8(3):234–242.
15. Baena E, Ortiz M, Martínez-A C, Moreno de Alborán I. c-Myc is essential for hematopoietic stem cell differentiation and regulates Lin-Sca-1+c-Kit- cell generation through p21. *Exp Hematol*. 2007;35(9):1333–1343.
16. Sheng Y, Ma R, Yu C, et al. Role of c-Myc haploinsufficiency in the maintenance of HSCs in mice. *Blood*. 2021;137(5):610–623.
17. Zanet J, Pibre S, Jacquet C, Ramirez A, Moreno de Alborán I, Gandarillas A. Endogenous Myc controls mammalian

epidermal cell size, hyperproliferation, endoreplication and stem cell amplification. *J Cell Sci*. 2005;118(8):1693–1704.
18. Bettess MD, Dubois N, Murphy MJ, et al. c-Myc is required for the formation of intestinal crypts but dispensable for homeostasis of the adult intestinal epithelium. *Mol Cell Biol*. 2005;25(17):7868–7878.
19. Davanger M, Evensen A. Role of the pericorneal papillary structure in renewal of corneal epithelium. *Nature*. 1971;229(5286):560–561.
20. Lavker RM, Sun TT. Epidermal stem cells. *J Invest Dermatol*. 1983;81(1 suppl):121s–127s.
21. Cotsarelis G, Cheng SZ, Dong G, Sun TT, Lavker RM. Existence of slow-cycling limbal epithelial basal cells that can be preferentially stimulated to proliferate: implications on epithelial stem cells. *Cell*. 1989;57(2):201–209.
22. Thoft RA, Friend J. The X, Y, Z hypothesis of corneal epithelial maintenance. *Invest Ophthalmol Vis Sci*. 1983;24(10):1442–1443.
23. Zadunaisky JA. Active transport of chloride across the cornea. *Nature*. 1966;209(5028):1136–1137.
24. Cao L, Zhang XD, Liu X, Chen TY, Zhao M. Chloride channels and transporters in human corneal epithelium. *Exp Eye Res*. 2010;90(6):771–779.
25. De Alboran IM, O'Hagan RC, Gärtner F, et al. Analysis of c-Myc function in normal cells via conditional gene-targeted mutation. *Immunity*. 2001;14(1):45–55.
26. Dassule HR, Lewis P, Bei M, Maas R, McMahon AP. Sonic hedgehog regulates growth and morphogenesis of the tooth. *Development*. 2000;127(22):4775–4785.
27. Grisanti L, Revenkova E, Gordon RE, Iomini C. Primary cilia maintain corneal epithelial homeostasis by regulation of the Notch signaling pathway. *Development*. 2016;143(12):2160–2171.
28. Stepp MA, Zieske JD, Trinkaus-Randall V, et al. Wounding the cornea to learn how it heals. *Exp Eye Res*. 2014;121:178–193.
29. Portal C, Rompolas P, Lwigale P, Iomini C. Primary cilia deficiency in neural crest cells models anterior segment dysgenesis in mouse. *eLife*. 2019;8:e52423.
30. Moyer PD, Kaufman AH, Zhang Z, Kao CW, Spaulding AG, Kao WW. Conjunctival epithelial cells can resurface denuded cornea, but do not transdifferentiate to express cornea-specific keratin 12 following removal of limbal epithelium in mouse. *Differentiation*. 1996;60(1):31–38.
31. Schindelin J, Arganda-Carreras I, Frise E, et al. Fiji: An open-source platform for biological-image analysis. *Nat Methods*. 2012;9(7):676–682.
32. Wang L, Cai W, Zhang W, et al. Inhibition of poly(ADP-ribose) polymerase 1 protects against acute myeloid leukemia by suppressing the myeloproliferative leukemia virus oncogene. *Oncotarget*. 2015;6(29):27490–27504.
33. Chin SS, Romano R-A, Nagarajan P, et al. Aberrant epidermal differentiation and disrupted ΔNp63/Notch regulatory axis in Ets1 transgenic mice. *Biol Open*. 2013;2(12):1336–1345.
34. Shu R, Bai D, Sheu T, et al. Sclerostin promotes bone remodeling in the process of tooth movement. *PLoS One*. 2017;12(1):e0167312.
35. Taketo M, Schroeder AC, Mobraaten LE, et al. FVB/N: an inbred mouse strain preferable for transgenic analyses. *Proc Natl Acad Sci USA*. 1991;88(6):2065–2069.
36. Wolosin JM, Alvarez LJ, Candia OA. Cellular pH and Na+-H+ exchange activity in lens epithelium of *Bufo marinus* toad. *Am J Physiol - Cell Physiol*. 1988;255(5):C595–C0623.
37. Wang Y, Chen M, Wolosin JM. ZO-1 in corneal epithelium; stratal distribution and synthesis induction by outer cell removal. *Exp Eye Res*. 1993;57(3):283–292.
38. Sokol JL, Masur SK, Asbell PA, Wolosin JM. Layer-by-layer desquamation of corneal epithelium and maturation of tear-facing membranes. *Invest Ophthalmol Vis Sci*. 1990;31(2):294–304.
39. Botchkarev VA, Flores ER. p53/p63/p73 in the epidermis in health and disease. *Cold Spring Harb Perspect Med*. 2014;4(8):a015248.
40. Soares E, Zhou H. Master regulatory role of p63 in epidermal development and disease. *Cell Mol Life Sci*. 2018;75(7):1179–1190.
41. Nagarajan P, Chin SS, Wang D, Liu S, Sinha S, Garrett-Sinha LA. Ets1 blocks terminal differentiation of keratinocytes and induces expression of matrix metalloproteases and innate immune mediators. *J Cell Sci*. 2010;123(20):3566–3575.
42. Williams SE, Beronja S, Pasolli HA, Fuchs E. Asymmetric cell divisions promote Notch-dependent epidermal differentiation. *Nature*. 2011;470(7334):353–358.
43. Okuyama R, Ogawa E, Nagoshi H, et al. p53 homologue, p51/p63, maintains the immaturity of keratinocyte stem cells by inhibiting Notch1 activity. *Oncogene*. 2007;26(31):4478–4488.
44. Di Iorio E, Kaye SB, Ponzin D, et al. Limbal stem cell deficiency and ocular phenotype in ectrodactyly-ectodermal dysplasia-clefting syndrome caused by p63 mutations. *Ophthalmology*. 2012;119(1):74–83.
45. Murray-Zmijewski F, Lane DP, Bourdon JC. p53/p63/p73 isoforms: an orchestra of isoforms to harmonise cell differentiation and response to stress. *Cell Death Differ*. 2006;13(6):962–972.
46. Dixon J, Dixon MJ. Genetic background has a major effect on the penetrance and severity of craniofacial defects in mice heterozygous for the gene encoding the nucleolar protein treacle. *Dev Dyn*. 2004;229(4):907–914.
47. Tanabe LM, Martin C, Dauer WT. Genetic background modulates the phenotype of a mouse model of dyt1 dystonia. *PLoS One*. 2012;7(2):e32245.
48. Doetschman T. Influence of genetic background on genetically engineered mouse phenotypes. *Methods Mol Biol*. 2009;530:423–433.
49. Sun P, Yuan Y, Li A, Li B, Dai X. Cytokeratin expression during mouse embryonic and early postnatal mammary gland development. *Histochem Cell Biol*. 2010;133(2):213–221.
50. Wolosin JM. Regeneration of resistance and ion transport in rabbit corneal epithelium after induced surface cell exfoliation. *J Membr Biol*. 1988;104(1):45–55.
51. Di Iorio E, Barbaro V, Ruzza A, Ponzin D, Pellegrini G, De Luca M. Isoforms of ΔNp63 and the migration of ocular limbal cells in human corneal regeneration. *Proc Natl Acad Sci USA*. 2005;102(27):9523–9528.
52. Yang A, Schweitzer R, Sun D, et al. P63 is essential for regenerative proliferation in limb, craniofacial and epithelial development. *Nature*. 1999;398(6729):714–718.
53. Pellegrini G, Dellambra E, Golisano O, et al. p63 identifies keratinocyte stem cells. *Proc Natl Acad Sci USA*. 2001;98(6):3156–3161.
54. Epstein SP, Wolosin JM, Asbell PA, Rapuano CJ. p63 expression levels in side population and low light scattering ocular surface epithelial cells. *Trans Am Ophthalmol Soc*. 2005;103:187–199.
55. Dingar D, Kalkat M, Chan PK, et al. BioID identifies novel c-MYC interacting partners in cultured cells and xenograft tumors. *J Proteomics*. 2015;118:95–111.
56. Vauclair S, Majo F, Durham AD, Ghyselinck NB, Barrandon Y, Radtke F. Corneal epithelial cell fate is maintained during repair by Notch1 signaling via the regulation of vitamin A metabolism. *Dev Cell*. 2007;13(2):242–253.
57. González S, Uhm H, Deng SX. Notch inhibition prevents differentiation of human limbal stem/progenitor cells in vitro. *Sci Rep*. 2019;9(1):10373.

Investigative Ophthalmology & Visual Science

58. González S, Halabi M, Ju D, Tsai M, Deng SX. Role of Jagged1-mediated Notch signaling activation in the differentiation and stratification of the human limbal epithelium. *Cells*. 2020;9(9):1945.
59. Movahedan A, Afsharkhamseh N, Sagha HM, et al. Loss of Notch1 disrupts the barrier repair in the corneal epithelium. *PLoS One*. 2013;8(7):e69113.
60. Ma A, Boulton M, Zhao B, Connon C, Cai J, Albon J. A role for notch signaling in human corneal epithelial cell differentiation and proliferation. *Invest Ophthalmol Vis Sci*. 2007;48(8):3576–3585.
61. Lu H, Lu Q, Zheng Y, Li Q. Notch signaling promotes the corneal epithelium wound healing. *Mol Vis*. 2012;18:403–411.
62. Robertson DM, Li L, Fisher S, et al. Characterization of growth and differentiation in a telomerase-immortalized human corneal epithelial cell line. *Invest Ophthalmol Vis Sci*. 2005;46(2):470–478.

Investigative Ophthalmology & Visual Science